

# Solar Photovoltaic Utilization in Electricity Generation to Tackle Climate Change

H. Demirhan<sup>1\*</sup>

<sup>1</sup> School of Science, Mathematical Sciences, RMIT University, Melbourne 3000, Australia

Received 25 May 2021; revised 01 February 2022; accepted 03 February 2022; published online 15 April 2022

**ABSTRACT.** Climate change is threatening nature by impacting the vital processes of life. The efforts to mitigate climate change mainly focus on utilizing renewable energy sources in high energy consumption areas. This article studies the contribution of solar photovoltaic (PV) utilization in electricity generation to climate change mitigation through a comprehensive modeling framework. The mean temperature anomalies, anthropogenic greenhouse gas emissions, solar photovoltaic capacity installations, and solar cycle length are considered using Australian data between 2001 and 2019. It is demonstrated that solar PV installations have a strong potential to contribute to mitigating climate change. A 1% increase in average PV installations contributes to reducing the temperature anomalies by 0.05%, and when considered in the same model with greenhouse gas emissions, a 1% increase in sunspot numbers increases temperature anomalies in Australia by 0.71% in the long-run. A low-magnitude relationship between solar cycle length and greenhouse gas emissions is also observed. The results of this study are beneficial in specifying more accurate targets, better allocation of limited climate action budgets, and better planning and management of solar energy investments.

*Keywords:* autoregressive distributed lag (ARDL) bounds testing, cointegration, greenhouse gas emissions, renewable energy, solar cycle, surface temperature anomalies

## 1. Introduction

New technologies and economic development lead to activities that increase electricity demand. Global primary energy consumption increased by 1.7% per year in the last decade (Zhang et al., 2019). Electricity and heat production share 25% of the generated greenhouse gas (GHG) emissions (Esen et al., 2017). Although energy consumption cannot be considered as the only reason for climate change or GHG emissions, the most significant part of GHG emissions is sourced from energy related anthropogenic activities, and it is considered to be the major thread to globalized human civilization in this century (Breyer et al., 2015; Elum and Momodu, 2017).

According to International Energy Agency, 28% of global energy generation was sourced from renewables in the first quarter of 2020. The share of solar photovoltaic (PV) systems in global electricity generation is almost 3% in 2020 (IEA, 2021), while PV generation can supply 30 ~ 50% of electricity in competitive markets (Creutzig et al., 2017). Findings in the recent literature show that independent of their scale, PV systems can contribute up to 55% over different long-run strategy scenarios (Breyer et al., 2015; Jäger-Waldau et al., 2020), although there are some obstacles to the propagation of solar PV generation (Shahsavari and Akbari, 2018). PV utilization in electricity gen-

eration has excellent potential to mitigate climate change. Its main contribution is to reduce GHG emissions and air pollution by generating almost zero carbon dioxide (CO<sub>2</sub>), nitrous oxide, methane gases, and waste products (Tsoutsos et al., 2005; Masson et al., 2014). Due to the strong correlation between GHG emissions and temperature anomalies (NOAA, 2021), lower GHG emissions translate into reduced temperature anomalies. The speed of increase in temperature anomalies is 0.22 °C/decade (Susskind et al., 2019), and two-third of the warming has occurred since the 1970s (NOAA, 2020), which show the swift response of the temperature anomalies to the changes in GHG emissions in a short period of time. This rapid relationship can also be seen in the mitigation of temperature anomalies by reducing GHG emissions. However, the relationship patterns between temperature anomalies, GHG emissions, and PV installations need to be figured out to understand the magnitude and speed of the mitigation in temperature.

In general, the contribution of solar energy utilization to the mitigation of climate change is investigated using indices or descriptive analyses without delving into the contribution of specific forms of solar energy utilization (Abdullah et al., 2014; Breyer et al., 2015; Shahsavari and Akbari, 2018; Jäger-Waldau et al., 2020). In this sense, there is insufficient information on the particular impact of solar PV capacity installations on temperature anomalies as a proxy of climate change. Revealing the amount of mitigating effect of solar PV installations on climate change is needed to set more achievable targets and strategies in climate emergency action plans and optimal use of economic resources to tackle climate change from the energy production

\* Corresponding author: Tel.: +61-03-99252729.  
E-mail address: haydar.demirhan@rmit.edu (H. Demirhan).

perspective. Due to the notable share of solar PV generation in the range of renewables, it is important to understand the contributions of solar PV utilization to the mitigation of climate change.

In the literature, the studies to model different proxies of climate change such as temperature anomalies employ Granger causality analysis, correlation/autocorrelation analysis, and linear and nonlinear lagged models (Fierro and Leslie, 2014; Breyer et al., 2015; Ayers, 2017; Muryshev et al., 2017; Booth, 2018; Hébert and Lovejoy, 2018). The long-run relationship between the concentration of CO<sub>2</sub> and global temperature is analyzed by using spectral density estimates, the Pearson correlation coefficient, and trend models (Davis, 2017). However, when working with time series data, the main source of information, namely autocorrelation in the series, needs to be considered by the employed statistical methods. In this sense, the use of a rolling correlation analysis can provide more accurate results than either the Pearson correlation coefficient or a non-parametric alternative. Furthermore, autoregressive distributed lag (ARDL) bounds testing approach (Pesaran et al., 2001), which tests for the spurious regression phenomena, has been used in climate modeling to explore long and short-run effects of various features on climate change. Although ARDL bounds and Granger causality analyses are used in climate research, to the best of our knowledge, only a limited number of studies focus on quantitatively estimating the contribution of solar PV utilization in electricity generation to the mitigation of climate change using these sophisticated modeling techniques.

This article studies the short- and long-run impact of average PV installations on climate change by using a comprehensive modeling framework that integrates the rolling correlations analysis, Granger causality analysis, and ARDL bounds testing. Having an insignificant signal between the dependent and exploratory series introduces the risk of discovering spurious relationships by ARDL bounds testing (Elkadhi et al., 2017; Emodi et al., 2018; Perez et al., 2018). Our modeling framework first statistically ensures that the signal between the pairs of dependent and exploratory series is significant using rolling correlation analysis. Since ARDL bounds testing is supported with Granger causality analysis, the likelihood of obtaining spurious relationships is minimized. A graphical approach for selecting lag orders of the Granger causality test is also introduced. Our modeling framework is suitable for any analysis that focuses on the short- and long-run relationship between climate change proxies and other exploratory features. The main practical contributions of this research are that i) the potential amount of reduction in temperature anomalies for every kW installed PV capacity is revealed. This is a crucial input for strategy making processes to mitigate climate change. ii) The impacts of 1% change in PV installations, 1% change in sunspot numbers, and one metric ton of carbon dioxide equivalent (Mt CO<sub>2</sub>-e) change in GHG emissions on the temperature anomalies are shown. iii) It is numerically demonstrated that solar cycle length needs to be considered in the climate change models through the existence of a significant signal between the pairs of sunspot numbers and GHG emissions and temperature anomalies, Granger causality between temperature anomalies and sunspot numbers, and long-run equilibrium relationship between GHG emissions

and sunspot numbers. Although sunspot numbers cannot be considered the primary source of climate change, their significant impact needs to be considered in climate related research.

## 2. Dataset and Methodology

### 2.1. Data and Overview of the Study System

In this study, the study system consists of Australia. According to the Australian National Greenhouse Gas Inventory, 33.3, 19.6, and 19.1% of GHG emissions in 2020 (excluding land-use, land-use change, and forestry emissions) were due to electricity generation, stationary energy, and transportation, respectively (DI, 2021b). In Australia, 7% of energy consumption was supplied from renewables in 2019 ~ 2020, and the shares of solar PV and solar hot water were 18.1 and 4.4%, respectively (DI, 2021a); hence, the share of solar PV generation is about 1.3% in the energy mix in Australia. In 2018 ~ 2019, the share of solar PV generation in renewables was 13.4% (DI, 2021a). This corresponds to an almost 5% increase in the share of PV generation in one year. It is projected that solar energy use in Australia will increase by 5.9% per year to 24 PJ in 2029 ~ 2030 (Bahadori and Nwaoha, 2013).

The observations of the study system are recorded over the timespan of September 2001 and June 2019. Summary statistics and 95% confidence intervals of mean for temperature anomalies, GHG emissions, PV installations, and sunspot numbers series are given in Table 1.

The main climate change proxy is the mean surface temperature anomaly that shows departures from the long-run average of surface temperature (Hébert and Lovejoy, 2018; Li et al., 2020; Valipour et al. 2021). The quarterly mean temperature anomalies series, which represents departures from the 1961 ~ 1990 average temperatures, is obtained from the Australian Government Bureau of Meteorology's Climate Change and Variability database (BOM, 2021a, 2021b). Consequently, this series meets the Australian Government Bureau of Meteorology data quality standards. The time series plot of the quarterly mean temperature anomalies series is given in Figure 1.

The temperature anomalies fluctuated around a mean level of 0.525 °C until Q3 of 2012. Then, the mean level shifted up to 1.122 °C between Q4 of 2012 and Q2 of 2019 as a strong impact of climate change. The overall mean of the temperature anomalies series was 0.749 °C with a 95% confidence interval of 0.602 and 1.929 °C. Such a wide confidence interval for the temperature anomalies is due to high positive and negative fluctuations resulting from climate change throughout September 2001 and June 2019. The mean temperature anomalies series is shown by  $\{T_t: t = 1, 2, \dots, 72\}$  and called "temperature anomalies series" throughout the article.

GHG emissions are recorded and maintained by the Australian Government Department of Industry, Science, Energy and Resources (DI). DI gets data from National Greenhouse Accounts that conform to the international guidelines of the United Nations Framework Convention on Climate Change and is subject to quality assurance processes to provide reliable data (DI, 2019). Quarterly GHG emissions series was obtained from

**Table 1.** Summary Statistics and 95% Confidence Intervals of Mean for Temperature Anomalies, GHG Emissions, PV Installations, and Sunspot Numbers Series

| Series                                | Min     | Median  | Mean    | Max     | SE     | 95% Confidence interval |         |
|---------------------------------------|---------|---------|---------|---------|--------|-------------------------|---------|
|                                       |         |         |         |         |        | Lower                   | Upper   |
| Temperature anomalies (°C)            | -0.870  | 0.748   | 0.749   | 2.120   | 0.075  | 0.602                   | 1.929   |
| GHG emissions (Mt CO <sub>2</sub> -e) | 130.600 | 141.200 | 142.100 | 157.700 | 1.013  | 140.115                 | 416.726 |
| PV installations (kW)                 | 12.3    | 10497.2 | 10026.1 | 50779.0 | 1263.3 | 7550.1                  | 24824.3 |
| Sunspot numbers                       | 2.767   | 49.583  | 60.829  | 187.433 | 5.975  | 49.118                  | 157.101 |

Note that SE represents standard error.

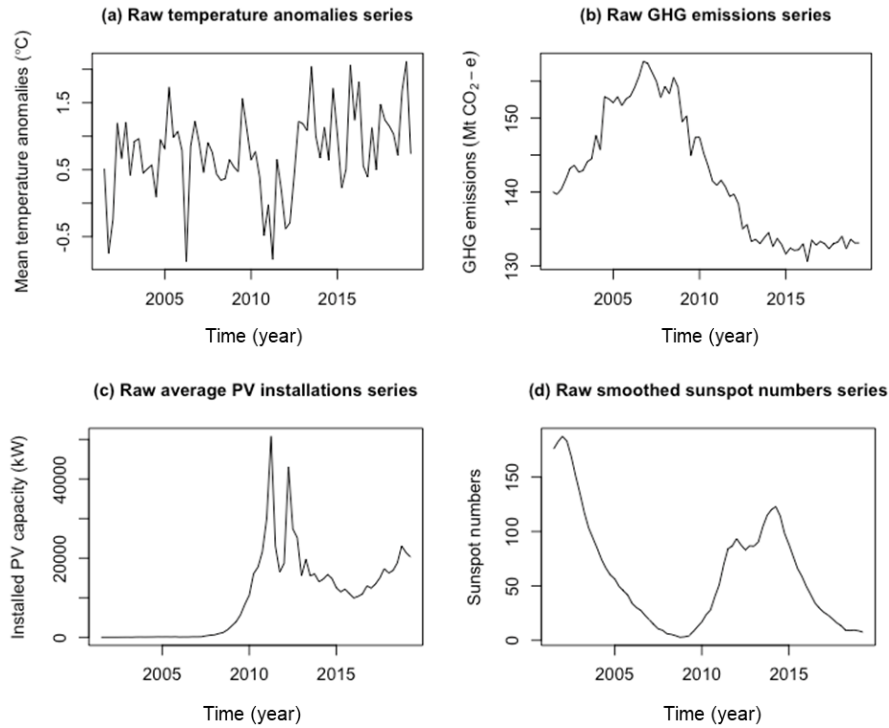


**Figure 1.** Time series plots of raw quarterly mean temperature anomalies, raw quarterly seasonally adjusted mean GHG emissions, raw quarterly average PV installations, and raw quarterly smoothed sunspot numbers series.

“Data Table 1B: Quarterly Emissions by Sector since 2001 ~ 2002, “Seasonally Adjusted” National Greenhouse Accounts Report (National Greenhouse Accounts, 2021). The average quarterly GHG emission in the observation period was 142.1 Mt CO<sub>2</sub>-e with a relatively small standard error (Table 1); hence, the range of GHG emissions in Australia over the observation period is also narrow. Raw quarterly seasonally adjusted GHG emissions series is plotted in Figure 1. There are multiple trends in the series as an indication of nonstationarity. Although the ARDL bounds test can be applied with nonstationary data, stationarity is needed for the Granger causality test. Since nonstationarity can cause discovering spurious relationships, the trend adjustment was applied to get both trend- and seasonally- adjusted GHG emissions series for the analysis. Adjustments were applied to other series for the same reason if the nonstationarity exists. For the adjustment, the Seasonal and Trend decomposition using Loess (STL) decomposition (Hyndman and Athanasopoulos, 2018) was used with the trend-cycle window of 13 and the seasonal window of 13. The time series plot of the ad-

justed GHG emissions series is given in Figure 2. After the adjustment, there is no evidence of either trend or seasonality in the GHG emissions series. The GHG emissions series is denoted by  $\{E_t: t = 1, 2, \dots, 72\}$  throughout the article.

The quarterly installed average PV capacity series was taken from the Australian Government Clean Energy Regulator (CER) database, and the quarterly mean installed average PV capacity series was calculated for our analysis. This database includes all the solar PV generator systems that have been installed under the Commonwealth Government’s Renewable Energy Target scheme (DI, 2018). Australian PV Institute publishes live and historical PV energy generation data from the CER’s databases. The series is published by Australian PV Institute (2021). CER applies thorough data quality control procedures through an online registry. The mean of quarterly average PV installations within the observation period was 100026.1 kW with a standard error of 1263.3 kW with an extremely large range and variation (Table 1). These statistics imply a large variation in the raw series displayed in Figure 1. There was a signi-

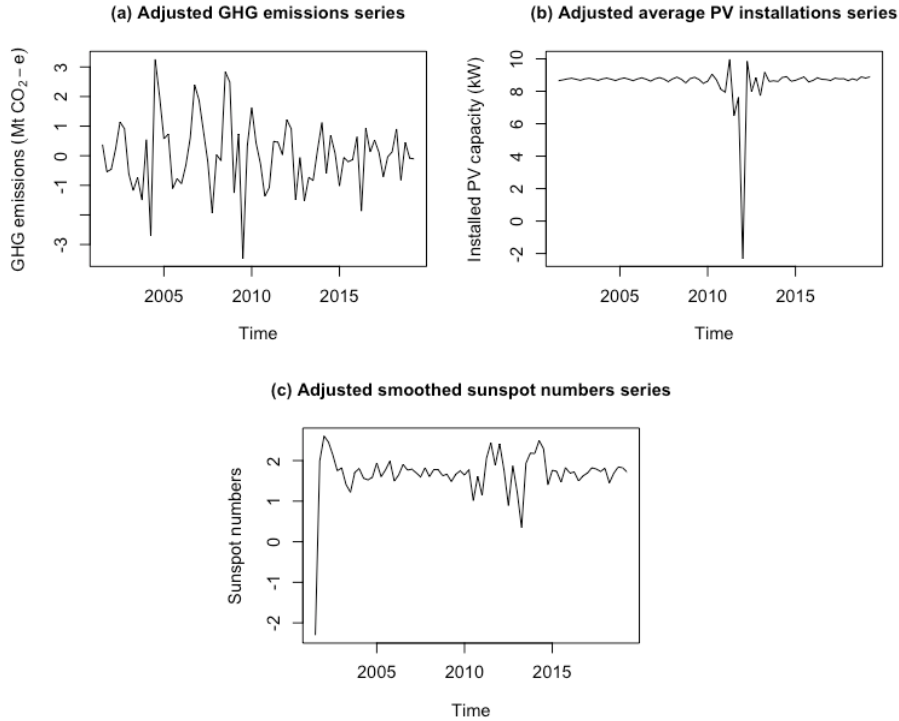


**Figure 2.** Time series plots of adjusted quarterly mean GHG emissions, log of adjusted quarterly PV installations, and log of adjusted quarterly smoothed sunspot numbers series.

ficant upward movement in 2010 based on the subsidies given by the Australian Government, such as the solar credit rebate scheme for PV installations. However, the average installed PV capacity came back to a mean level, which was significantly higher than the level before 2010 and showed a slightly upward trend after 2015. This series was adjusted for trend using the STL decomposition with the trend-cycle window of 5 and the seasonal window of 13 to remove the nonstationarity. The logarithmic transformation was also applied to reduce the variance of PV installations series due to large fluctuations between 2010 and 2012. The adjusted average PV installations series is denoted by  $\{P_t; t = 1, 2, \dots, 72\}$  throughout the article. Since there are negative values in  $P_t$  series,  $\log(P_t + |\min(P_t)| + 0.1)$  was used, where  $|\cdot|$  is the absolute value of the inner expression for the logarithmic transformation. The time series plot of the adjusted quarterly log-average PV installations series is shown in Figure 2. The drop around 2010 ~ 2012 is due to the explosive increase in the raw PV installations series around the same time-frame.

Solar cycle lengths have been used as a predictor for the surface temperature and its anomalies in the literature. An inverse relationship was observed between solar cycle lengths and surface temperatures (Friis-Christensen and Lassen, 1991; Lassen and Friis-Christensen, 1995, 2000; Solheim et al., 2012). Solar cycle length is used to predict global average surface temperature anomaly along with  $\text{CO}_2$  by using the sunspot numbers as the proxy of solar cycle lengths to give temperature anomaly forecasts for a horizon up to 2100 (Kristoufek, 2017; Booth, 2018). The study of Booth (2018) established significant evidence for the impact of solar cycle length on transient climate re-

sponse. The sunspot numbers series used in this study originated from the U.S. Department of Commerce, National Oceanic and Atmospheric Administration (NOAA), Space Weather Prediction Center (SWPC), Space Weather Operations (SWO) Unit (SWPC NOAA, 2021). The dataset was published by SWPC NOAA (2021) in monthly average daily sunspot numbers. The data quality is subject to the data quality assurance procedures of NOAA. The smoothed monthly series was converted into quarterly series as displayed in Figure 1 to get quarterly average daily smoothed sunspot numbers series. The sunspot numbers have an approximately a cycle of approximately 11 years (Singh et al., 2011). In the considered time period, they had a peak in the Q1 of 2002 and then a dip in Q4 of 2008, another peak around 2014. On the other hand, GHG emissions made a peak in Q3 of 2008 and a dip in Q2 of 2014. From the descriptive analysis perspective, there is a counter-movement in sunspot numbers and GHG emissions over the same time-frame. This is a descriptive indication of a significant relationship between these two series, which is explored in detail in Section 3.1. From Table 1, the mean of average daily smoothed sunspot numbers was 60.83 with a standard error of 5.97 with a large range and variation. Since the raw series displays multiple trends, the stationarity of the series needs to be ensured. A trend adjustment was made using STL decomposition with the trend-cycle window of 7 and the seasonal window of 13. The quarterly average daily sunspot numbers series is shown by  $\{S_t; t = 1, 2, \dots, 72\}$  and called “sunspot numbers series” (SSN) throughout the article. The logarithmic transformation was applied to stabilize the adjusted series as much as possible using the formula  $\log(S_t + |\min(S_t)| + 0.1)$  due to the negative values

in the adjusted series. The time series plot of the adjusted quarterly sunspot numbers series is shown in Figure 2. After the adjustment, the periodicity of sunspot numbers is not seen within the considered time window.

The analysis of solar PV utilization's impact on the temperature anomalies requires simultaneous data on exploratory variables and the dependent variable in the same frequency, at least on the Australia scale. Also, the data need to be going through a quality control process of the data provider. For the analysis presented in this study, other variables from weather and solar energy utilization data would also be thought of as explanatory variables. However, to the best of our knowledge, quarterly solar thermal systems data is unavailable for Australia from the third quarter of 2001 to the second quarter of 2019. PV data is the only available solar energy utilization data that goes through a quality control process and is available in quarterly frequency over the study's timespan.

A missing model component distracts the assumptions of the model, such as the randomness of residuals. The information in the dependent variable not captured by a model (a function of explanatory variables) goes to the residuals. Therefore, the suitability of a model and the sufficiency of explanatory variables are assessed by residual analysis. The primary source of information in time series data is the autocorrelation in the dependent variable. So, the impact of a missing explanatory variable(s) is observed in the residual analysis by seeing a significant autocorrelation in residuals which is not captured by the model and nonnormality of the residuals. In our case, it is demonstrated that there is no residue autocorrelation left in residuals, and they are normally distributed as expected in Section 3. This implies that the model captures all the information in the dependent variable; hence, the current exploratory variables provide the model with sufficient explanatory capacity to acquire the variation in the temperature anomalies. Therefore, not having another solar variable does not impact the generalizability of the work. Another consideration for including other weather and solar variables in the same analysis with PV installations is that it would create misleading results due to multicollinearity. Thus, in this work, the impact of PV installations is solely focused on among many other solar energy-related series. Full dataset and R codes for implementing all the time series adjustments and analyses in the article are given in the Electronic Supplementary Material.

## 2.2. Rolling Correlation Analysis

It is essential to ensure that the signal in the series is significantly different from pure random noise or not dominated by the physical variabilities, especially when the series is relatively short or includes low-frequency data. The rolling correlation analysis proposed by Gershunov et al. (2001) is implemented to check if the signals can significantly be distinguished from the white noise. The null hypothesis of the test is that "the signals in a pair of series are not significantly different from the white noise." In this approach, standard deviations of empirical rolling correlations of two original series and those of two correlated white noise series at the same magnitude as the original series are com-

pared by simulating the white noise series many times. Since the white noise series are replicated many times, the  $(1 - \alpha)\%$  level confidence limits are produced for the standard deviation of rolling correlations in the white noise series. Then, if the empirical standard deviation of rolling correlations is between the confidence limits, it is concluded that there is no significant difference between the signals in the series and the white noise. On the other hand, it is decided that the correlation between the series is physical if the empirical standard deviation is outside the confidence limits (Gershunov et al., 2001). The "rolCorPlot" function from the "dLagM" R package (version 1.1.3) is used to implement this test (Demirhan, 2020).

## 2.3. Unit-Root and Granger Causality Testing

A time series is either trend- or difference-stationary. If the series is trend-stationary, removing the trend makes the series stationary. Whereas, if the series is difference-stationary, it is integrated of order  $d$ , i.e.  $I(d)$ , and taking the  $d$ -th difference of the series makes it stationary. To check for the stationarity of the series, Augmented Dickey-Fuller (ADF), Phillips-Perron (PP), and Kwiatkowski-Phillips-Schmidt-Shin (KPSS) unit-root tests are employed using the R package "urca" (Said and Dickey, 1984; Kwiatkowski et al., 1992; Banerjee et al., 1993; Cryer and Chan, 2008; Pfaff, 2008). The null hypothesis of the ADF and PP tests is that "a unit-root is present in the time series". Whereas the null hypothesis of the KPSS test states that "the time series is trend-stationary".

Due to a numerical linear relationship between two nonstationary series, a spurious correlation can be obtained between them. This implies the impracticality of using the exploratory series  $\{X_t\}$  in forecasting the dependent series  $\{Y_t\}$ . Granger test of causality is a statistical procedure to test if  $\{X_t\}$  series is useful in forecasting  $\{Y_t\}$  series (Granger, 1969). The null hypothesis of the Granger causality test is that " $\{X_t\}$  does not Granger cause  $\{Y_t\}$ ". The most critical input of this test is the number of lags of  $\{X_t\}$  and  $\{Y_t\}$  series included in the model (Thornton and Batten, 1985). Two linear models are constructed to implement the Granger test based on pre-specified lag orders of  $\{X_t\}$  and  $\{Y_t\}$  series. The lag orders determine the number of parameters in the models, creating a trade-off between the bias created by a parsimonious parameterization and inefficiency due to overparameterization. This trade-off is addressed by using information criteria (Thornton and Batten, 1985). The number of lags can be specified by using information criteria such as Akaike Information Criterion (AIC) or Bayesian Information Criterion (BIC) (Akaike, 1970; Geweke and Meese, 1981). While AIC penalizes the log-likelihood by the number of parameters in the model, BIC simultaneously considers the number of parameters in the model and the sample size. AIC and BIC tend to favour a large lag order for small to moderate samples, hence, a false-positive Granger causality finding (Bruns and Stern, 2019). In this sense, considering only one lag order based on either AIC or BIC is a restrictive approach and frequently generates false-positive findings in the literature that focuses on Granger causality between energy use and economic output (Bruns and Stern, 2019). On the other hand, researchers can consider running multiple Granger tests with different lag lengths and use only the

ones that reject the null hypothesis of the Granger test, which is called “*p*-hacking” and has the potential to produce excess significance (Bruns and Stern, 2019). To avoid excess significance, the lag order for the Granger test is selected by visualizing the *p*-values computed for many lags along with the corresponding rescaled AIC and BIC values in the same plot. Rescaling is done by dividing AIC or BIC values by their maximum for plotting purposes. Instead of selecting the lag order that gives significant causality (to avoid “*p*-hacking”), the lags corresponding to the notable drops in both or either of AIC and BIC over all the plotted ranks are considered and the corresponding *p*-values are taken into account for the test. A drop in the information criteria implies that the bigger model where the drop occurs provides us with a notably better model in terms of the goodness-of-fit since the increase in the goodness-of-fit dominates the penalty applied by the information criteria due to the increasing size of the model. Accordingly, a significant *p*-value implies that the corresponding lag order can be used for testing. We do not straightforwardly go for the minimum AIC or BIC in this approach. Instead, we look for a notable drop that indicates a considerable improvement in the goodness-of-fit before reaching out to large lag orders, which is the main reason for overfitting caused by the use of information criteria. This approach can be further investigated in terms of its sensitivity and specificity in hypothesis testing. However, this is outside the scope of this study.

The “grangertest” function from the R package “lmtest” is used to implement the Granger causality test (Zeileis and Hothorn, 2002). The code to create the mentioned visualization is given in Section 2.5 of the Electronic Supplementary Material.

## 2.4. ARDL Bounds Testing

ARDL models allow the inclusion of independent time series into autoregressive models. Cointegration analysis is used to assess the short- and long-run relationships between a dependent series and a set of independent series (Pesaran et al., 2001). ARDL bounds testing approach proposed by Pesaran et al. (2001) provides a practical way of conducting the cointegration analysis. The stationarity of the series is one of the major considerations in cointegration analysis (Pretis and Hendry, 2013). In this sense, the ARDL bounds test can be applied with nonstationary series provided that they are  $I(1)$ . ARDL bounds testing is more robust to a small sample size than its counterparts (Zhai et al., 2017). This makes it reliable to run a cointegration analysis with a relatively shorter series (Zhai et al., 2017). It also provides short- and long-run relationships simultaneously by one analysis (Zhai et al., 2017). Pesaran et al. (2001) defined five different settings for the structure of constant and trend in the equilibrium relationship. The details of the test and its implementation are given in Section 1 of the Electronic Supplementary Material. The ARDL bounds test is conducted based on an *F*-statistic under the null hypothesis that “there is no cointegration among the series” against the alternative hypothesis stating the existence of cointegration. If a significant cointegration is identified, then the general error correction model (ECM) given in Equation (S2) of the Electronic Supplementary Material is fit-

ted to figure out the long-run equilibrium relationship between the series and their short-run effects on temperature anomalies.

## 2.5. Modeling Framework

The proposed modeling framework integrates rolling correlations analysis, Granger causality tests, and ARDL bounds testing into a framework to demonstrate the relationship patterns between temperature anomalies, GHG emissions, sunspot numbers, and PV utilization. The flow diagram of the modeling framework proposed in this study is given in Figure 3. The analysis starts with a descriptive analysis of the dataset, including testing the significance of signal between pairs of dependent and exploratory series. If the signal is significant, then the analysis continues in two arms: i) implementing the Granger causality test at many lag orders and ii) investigating if all the series are integrated of the maximum order of one. In the first arm of the analysis, the *p*-values of Granger causality tests, rescaled AIC, and rescaled BIC are displayed in a plot, and the *p*-value where a drop occurs in AIC and/or BIC is taken to decide the significance of the Granger causality. If the Granger causality is significant, the Granger causality test results are merged with ARDL bounds testing to specify the ARDL model used in ARDL bounds testing. Also, the results of Granger causality tests are interpreted to draw conclusions. In the second arm of the analysis, if all the series are integrated of the maximum order of one, the ARDL models are specified as the next step where the two arms of the analysis intersect. Then, the lag orders are specified, and the ARDL bounds testing is carried on. The essential step of the framework is the diagnostic checking of the model assumptions. The serial independence of residuals, homoscedasticity of residuals, normality of residuals, the correctness of the model’s functional form for the lag orders of the test, and stability of residuals are demonstrated for the validity of the ARDL bounds test results. If all the assumptions are validated, the analysis is terminated by interpreting all the results in relation to the research questions. Suppose there is an insignificant signal, higher orders of integration, or violation of assumptions in the flow. In that case, we need to terminate the analysis and go back to the dataset to fix the issue.

From Figure 3, after a descriptive analysis such as in Section 2.1, we first need to demonstrate that the correlation patterns between the dependent and exploratory series, namely the signals between the pairs of the series, are significantly different from random noise. The rolling correlation analysis of Gershunov et al. (2001) is used for this purpose. This step ensures that there is significant information to be captured by modeling and helps the practitioner to avoid detecting spurious relationships. Then, Granger causality tests are implemented by making the selection based on the changes in AIC and BIC, as explained in Section 3.2. This way, we aim to avoid detecting spurious relationships. In parallel, the unit root tests are implemented to ensure the main assumption of ARDL bounds testing that the series are integrated up to a maximum order of one. For the specification of the model that involves deciding on the exploratory series to be included in the model, significant Granger causalities between the dependent and the exploratory se-

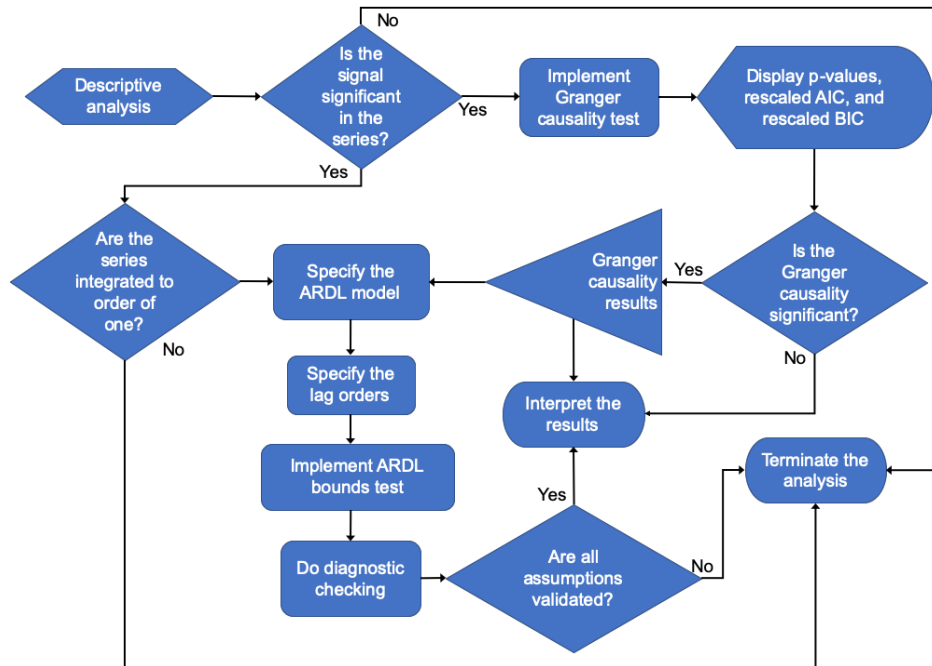


Figure 3. Flow diagram of the modeling framework.

ries are considered. The search algorithm of Demirhan (2020) is employed to specify the lag orders for the series in the model. After implementing the ARDL bounds test, we need to ensure that none of the assumptions of the ARDL bounds test is violated through a comprehensive diagnostic checking. The outputs of both ARDL bounds and Granger causality tests are considered simultaneously to draw inferences.

### 3. Results

#### 3.1. Rolling Correlation Analysis

The rolling correlation analysis is implemented to analyze the correlation structure between two time series over different time windows. This analysis is used to test if the signals in the pairs of  $\{T_t, E_t^*\}$ ,  $\{T_t, P_t^*\}$ , and  $\{T_t, S_t^*\}$  series are significantly different from the white noise series or not (Gershunov et al., 2001). Since the logarithmic transformation changes the correlation structure of the series, raw series  $E_t^*$ ,  $P_t^*$ , and  $S_t^*$  are used for the rolling correlations analysis in this section. In the rolling correlation analysis, a narrow window length examines the signal for closer quarters, and a wide window length covers the correlation over several years. Since the length of the series is not relatively long, a large window length is not suitable for the analysis. The window lengths of 5, 7, 11, 15, and 17 were taken to cover small, moderate, and relatively large windows for testing. Figure 4 shows the rolling correlations between the pairs of  $\{T_t, E_t^*\}$ ,  $\{T_t, P_t^*\}$ ,  $\{T_t, S_t^*\}$ , and  $\{E_t^*, S_t^*\}$ . In Figure 4, the dashed red lines show the 95% confidence interval limits for the mean of the average rolling correlations indicated by the horizontal solid line. The bold, solid line shows the average rolling correlation over the widths.

The rolling correlations between temperature anomalies and

GHG emissions came down to low levels from moderate to high at the beginning of the 2000s. Then, an increase to a positive and moderate level was seen around 2012. The overall average rolling correlation hit a negative, moderate-to-high level before 2015 and shifted towards positive values by 2020. This can be due to the impact of another variable and efforts made to mitigate the temperature anomalies. The rolling correlations between temperature anomalies and PV installations in Australia navigated up and down in a range of moderate-to-low positive and negative correlations until 2010. Due to the enormous increase in the investments in the utilization of solar radiation as a renewable energy source in 2010, the rolling correlation patterns jumped to a negative moderate-to-high value and had remained there for almost four years. This implies the mitigating potential of solar investments on temperature anomalies. Then, possibly due to the reduced rate of increase in average PV installations, a decrease in the magnitude of the rolling correlations towards a positive, low-to-moderate level was observed by 2020. The rolling correlations between temperature anomalies and SSN fluctuated between negative and positive moderate levels until 2012, and after a drop-down to  $-0.7$  level, it decreased in magnitude and continued to swing around low levels of rolling correlation. A moderate negative overall rolling correlation was observed between GHG emissions and SSN. The correlation between GHG emissions and SSN within a one- to two-year window rose to a very high magnitude around 2010 and 2014, where these series had almost opposite trends (Figure 1). This strongly indicates a significant relationship between GHG emissions and a non-anthropogenic feature SSN.

To test the significance of signals between the considered pairs of temperature anomalies and the exploratory features, standard deviations of rolling correlations and corresponding 95%

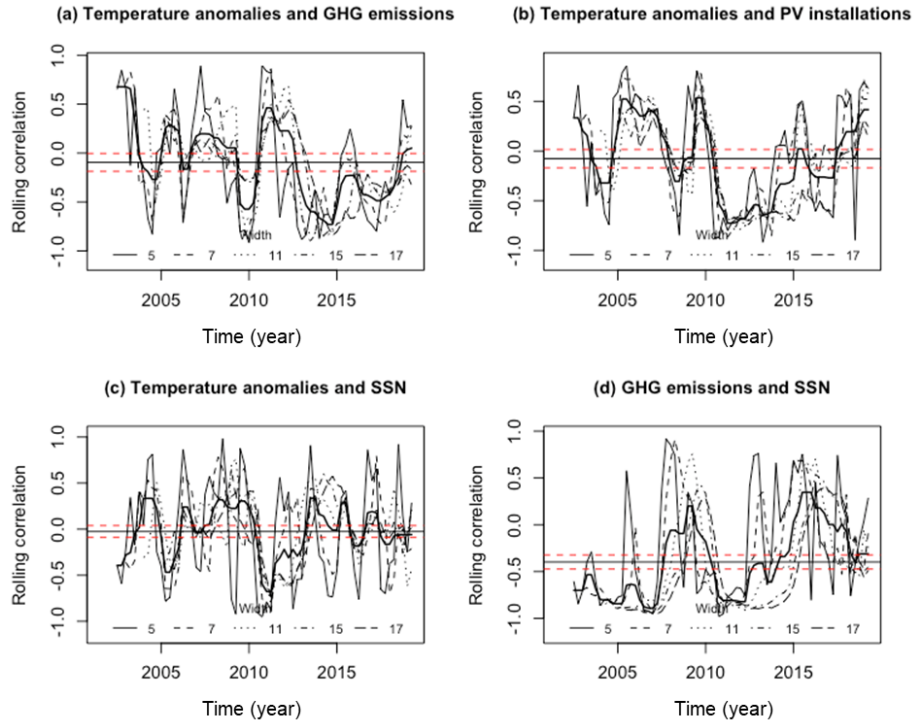


**Figure 4.** Rolling correlations between temperature anomalies and GHG emissions, PV installations, and SSN series for the window lengths of 5, 7, 11, 15, and 17. Flat black and red lines show the overall mean level and the corresponding 95% confidence interval.

test limits for all pairs and 90% test limits for the pair of temperature anomalies – SSN are given in Table 2. At a 5% level of significance, the signals between temperature anomalies and GHG emissions and those between temperature anomalies and PV installations are significant for the widths of 7, 11, 15, and 17. The rolling correlations between GHG emissions and SSN are significant for all window widths. Those between temperature anomalies and SSN are significant at a 5% level of significance for the window width of 5 and at a 10% level of significance for the widths of 11, 15, and 17. Overall, it is concluded that the signals between the pairs of  $\{T_t, E_t^*\}$ ,  $\{T_t, P_t^*\}$ ,  $\{T_t, S_t^*\}$ , and  $\{E_t^*, S_t^*\}$  are all significantly different from the white noise characteristic.

This result implies that using temperature anomalies series as a dependent feature and GHG emissions, PV installations, and SSN series as exploratory features for further analyses is suitable. Based on the significance of the signal between GHG emissions and the SSN series, analysis of the relationship between these series is applicable. Therefore, it is safe to proceed to the next Granger causality analysis step and assess the degree of integration in the proposed modeling framework in Figure 3.

### 3.2. Degree of Integration

The results of unit-root tests applied to ensure temperature anomalies and the adjusted GHG emissions, PV installations, and SSN series are either  $I(0)$  or  $I(1)$  are given in Table 3. It is concluded that at a 5% level of significance that there is no unit root for the temperature anomalies, GHG emissions, PV installa-

tions, and SSN series ( $I(0)$ ) by ADF, PP, and KPSS tests; hence, the main assumption of the ARDL bounds test is satisfied. Based on these results, it is appropriate to proceed with the model specification for ARDL bounds testing as per the proposed modeling framework in Figure 3.

### 3.3. Granger Causality Analysis

Since the Granger causality test is sensitive to the choice of the lag orders, instead of reporting a single  $p$ -value for a predetermined lag order,  $p$ -values of the Granger causality test and rescaled AIC and BIC values are plotted for a range of lag orders in Figure S2 Supplementary Material for the  $\{Y_t, X_t\}$  pairs of  $\{T_t, E_t\}$ ,  $\{T_t, P_t\}$ ,  $\{T_t, S_t\}$ ,  $\{E_t, T_t\}$ ,  $\{E_t, S_t\}$ , and  $\{P_t, T_t\}$ . Following the Granger test arm of the modeling flow in Figure 3, AIC and BIC values are rescaled by dividing to their maximum over the considered range of lag orders to plot AIC and BIC values next to the  $p$ -values. From Figure S2, it is expected to see a significant  $p$ -value ideally for the lag where a drop occurs in AIC and/or BIC to decide the significance of the Granger causality. Accordingly, there is a significant Granger causality between temperature anomalies and GHG emissions (Panel (a)), temperature anomalies and SSN (Panel (e)), and PV installations and temperature anomalies (Panel (d)). GHG emissions and SSN contain useful information to forecast temperature anomalies, which can also be used to forecast PV installations. This result follows from the increasing PV investments to mitigate climate change. For the test between temperature anomalies and PV installations (Panel (c)),  $p$ -values that are close to the 10% significance level are seen at lags 10 and 17.

There are also many significant lags, including the one that corresponds to the minimum BIC value for the test between PV installations and temperature anomalies (Panel (d)). This indicates the existence of Granger causality between temperature anomalies and PV installations. There is no evidence of the usefulness of temperature anomalies and PV installations in forecasting GHG emissions (Panel (b) and (g)). The Granger causality test barely identifies a causality between GHG emissions and SSN at the 10% significance level (Panel (f)). Significant rolling correlations are observed between these series within sub-intervals of the considered timespan. However, the SSN series is mildly informative for forecasting GHG emissions over the whole time-span of the study. GHG emissions include some information to predict PV installations (Panel (g)). This result would be due to the reactional PV installations to increasing GHG emission levels.

**Table 2.** Standard Deviations of Rolling Correlations and Corresponding Test Limits for the Pairs of Temperature Anomalies, GHG Emissions, PV Installations, and SSN

| Pair                                       | Width | Sd. Rol. Cor. | 95% limit | 5% limit  |
|--|-------|---------------|-----------|-----------|
| Temperature anomalies and GHG emissions    | 5     | 0.526         | 0.552     | 0.407     |
|  | 7     | 0.480         | 0.467     | 0.307     |
|  | 11    | 0.441         | 0.370     | 0.204     |
|  | 15    | 0.355         | 0.325     | 0.155     |
|  | 17    | 0.351         | 0.301     | 0.136     |
| Temperature anomalies and PV installations | 5     | 0.549         | 0.559     | 0.423     |
|  | 7     | 0.504         | 0.474     | 0.320     |
|  | 11    | 0.438         | 0.383     | 0.213     |
|  | 15    | 0.381         | 0.329     | 0.162     |
| GHG emissions and SSN                      | 5     | 0.581         | 0.530     | 0.414     |
|  | 7     | 0.529         | 0.437     | 0.311     |
|  | 11    | 0.510         | 0.349     | 0.220     |
|  | 15    | 0.483         | 0.297     | 0.169     |
| Temperature anomalies and SSN              | 5     | 0.567         | 0.559     | 0.418     |
|  | 7     | 0.446         | 0.473     | 0.316     |
|  | 11    | 0.357         | 0.381     | 0.213     |
|  | 15    | 0.317         | 0.326     | 0.160     |
|  | 17    | 0.312         | 0.308     | 0.146     |
|  | Width | Sd. Rol. Cor. | 90% limit | 10% limit |
| Temperature anomalies and SSN              | 5     | 0.567         | 0.537     | 0.429     |
|  | 7     | 0.446         | 0.451     | 0.324     |
|  | 11    | 0.357         | 0.356     | 0.226     |
|  | 15    | 0.317         | 0.306     | 0.173     |
|  | 17    | 0.312         | 0.287     | 0.158     |

Sd. Rol. Cor.: Standard deviations of rolling correlations; significant standard deviations are marked bold.

Overall, since Granger causalities are found between pairs of temperature anomalies and GHG emissions, SSN and PV installations, and between GHG emissions and SSN, it is suitable to include GHG emissions, SSN, and PV installations in ARDL bounds testing for the dependent feature temperature anomaly.

Also, SSN contains useful information to explain GHG emissions over an ARDL bounds testing. Due to the significance of the signal and Granger causalities between the temperature anomalies and exploratory series, we proceed with ARDL bounds testing as per the modeling framework of Figure 3.

**Table 3.** P-Values of the ADF, PP, and KPSS Unit Root Tests for the Considered Series

| Test | $T_t$  | $E_t$  | $P_t$  | $S_t$  |
|------|--------|--------|--------|--------|
| ADF  | < 0.01 | < 0.01 | < 0.01 | < 0.01 |
| PP   | < 0.01 | < 0.01 | < 0.01 | < 0.01 |
| KPSS | > 0.10 | > 0.10 | > 0.1  | > 0.1  |

$T_t$ : Temperature anomalies series;  $E_t$ : GHG emissions series;  $P_t$ : PV installations series;  $S_t$ : Sunspot numbers series.

### 3.4. Short and Long Run Relationships

#### 3.4.1. Temperature Anomalies

The lag structure of the ARDL model in Equation (S1) of Supplementary Material needs to be specified to apply the ARDL bounds test. For this aim, AIC or BIC was minimized using the search algorithm proposed by Demirhan (2020) using the “ardl-BoundOrders” function from the “dLagM” package. The maximum lag order was set to 5 to define the search domain for optimal AIC or BIC. The maximum lag order was selected based on the sample size and parsimony principle to avoid over-fitting (Parzen, 1982). Any increase in the number of lags included in a model raises the number of parameters. When we have a model with large lag orders, a large sample is needed to inform the parameters in the model to get reliable results. A large number of lag orders also creates extreme learning from the data and results in an over-fitting, non-parsimonious model. AIC penalizes models with the number of parameters, and BIC penalizes the models considering both the sample size and the number of parameters. In this sense, large lags relative to the sample size are expected to be eliminated by BIC. Setting a high maximum lag order increases the risk of getting a non-parsimonious model and increases the search time by spending computation time on less likely models. Optimizing AIC led to  $p_T = 0$  and  $p_E = 0$ ,  $p_P = 5$ , and  $p_S = 4$ , namely ARDL(0, 0, 5, 4), as the best model and ARDL(0, 0, 5, 0) as the second-best model. Whereas BIC gave ARDL(0, 0, 0, 0) as the best model and ARDL(0, 0, 5, 0) as the second-best. Since ARDL(0, 0, 0, 0) does not include any short term impact of any of the variables and considering the agreement between AIC and BIC and the parsimony principle, the orders were set as follows:  $p_T = 0$  and  $p_E = 0$ ,  $p_P = 5$ , and  $p_S = 0$  for the lag structure of the ARDL bounds test. Based on the specified orders, four past quarters were considered for PV installation series in Equation (S1) of the Supplementary Material; and hence, the duration of short-run is under 4 for this data, and that of long-run is longer than a year. The ARDL bounds test results and the tests for violations of assumptions and AIC and BIC of the general ECM under each case are given by Table 4, where significant  $F$ -statistics and the smallest values AIC and BIC are bold-faced.

The serial independence of the residuals is confirmed by BG and LB tests under the null hypothesis that “there is no se-

**Table 4.** Results of ARDL Bounds Test, Diagnostic Tests for the Model Assumptions, and AIC and BIC, of the Full Model for All Cases

|        | Critical values for the <i>F</i> -Test |              |              | <i>F</i> -Stat. | <i>P</i> -values of the tests for assumptions |       | GOF measures for the full model |        |
|--------|--|--------------|--------------|-----------------|---|-------|---------------------------------|--------|
|        | Sig. Level                             | <i>I</i> (0) | <i>I</i> (1) |                 |   |       |                                 |        |
| Case 1 | 10%                                    | 2.010        | 3.100        | 6.319**         | BG  | 0.473 | AIC                             | 119.08 |
|        | 5%                                     | 2.450        | 3.630        |                 | LB  | 0.705 | BIC                             | 147.54 |
|        | 1%                                     | 3.420        | 4.840        |                 | BP  | 0.992 |                                 |        |
|        |  |              |              |                 | SW  | 0.186 |                                 |        |
|        |  |              |              |                 | RESET   | 0.829 |                                 |        |
| Case 2 | 10%                                    | 2.482        | 3.334        | 5.513**         | BG  | 0.469 | AIC                             | 121.07 |
|        | 5%                                     | 2.946        | 3.862        |                 | LB  | 0.703 | BIC                             | 151.73 |
|        | 1%                                     | 4.048        | 5.092        |                 | BP  | 0.934 |                                 |        |
|        |  |              |              |                 | SW  | 0.198 |                                 |        |
|        |  |              |              |                 | RESET   | 0.828 |                                 |        |
| Case 3 | 10%                                    | 2.838        | 3.898        | 6.200**         | BG  | 0.469 | AIC                             | 121.07 |
|        | 5%                                     | 3.408        | 4.550        |                 | LB  | 0.703 | BIC                             | 151.73 |
|        | 1%                                     | 4.725        | 6.080        |                 | BP  | 0.934 |                                 |        |
|        |  |              |              |                 | SW  | 0.198 |                                 |        |
|        |  |              |              |                 | RESET   | 0.753 |                                 |        |
| Case 4 | 10%                                    | 3.110        | 3.900        | 6.015**         | BG  | 0.462 | AIC                             | 119.59 |
|        | 5%                                     | 3.624        | 4.488        |                 | LB  | 0.690 | BIC                             | 152.43 |
|        | 1%                                     | 4.808        | 5.786        |                 | BP  | 0.802 |                                 |        |
|        |  |              |              |                 | SW  | 0.699 |                                 |        |
|        |  |              |              |                 | RESET   | 0.682 |                                 |        |
| Case 5 | 10%                                    | 3.618        | 4.635        | 6.764*          | BG  | 0.438 | AIC                             | 119.59 |
|        | 5%                                     | 4.253        | 5.363        |                 | LB  | 0.690 | BIC                             | 152.43 |
|        | 1%                                     | 5.698        | 6.970        |                 | BP  | 0.802 |                                 |        |
|        |  |              |              |                 | SW  | 0.699 |                                 |        |
|        |  |              |              |                 | RESET   | 0.681 |                                 |        |

\* Significant at 5% level of significance. \*\* Significant at 1% level of significance. BG: Breusch-Godfrey test (Asteriou and Hall, 2021). LB: Ljung-Box test (Cryer and Chan, 2008). BP: Breusch-Pagan test (Asteriou and Hall, 2021). SW: Shapiro-Wilk test (Cryer and Chan, 2008). RESET: Ramsey's RESET test (Asteriou and Hall, 2021).

rial correlation in the series”, homoscedasticity of the residuals is confirmed by BP test under the null hypothesis that “the residuals are homoscedastic”, and normality of residuals is confirmed by SW test under the null hypothesis that “the residuals are normally distributed” with all *p*-values greater than 0.05. And there is no issue around the correctness of the model’s functional form for all cases by Ramsey’s RESET test under the null hypothesis that “there is no specification issue with the linear form of the model” with all *p*-values greater than 0.05. For Cases 1 to 4, there is evidence to conclude the existence of cointegration between temperature anomalies and GHG emissions, PV installations, and sunspot numbers at a 1% level of significance, whereas the same is concluded at a 5% level with Case 5. So, there is a statistically significant long-run relationship (equilibrium) between temperature anomalies and GHG emissions, PV installations, and sunspot numbers series in Australia.

Since both AIC and BIC suggest Case 1, the results with Case 1 are reported in detail. In order to check the stability of the model, the cumulative sum (CUSUM), the cumulative sum of squared recursive residuals (CUSUMSQ), and the moving sum (MOSUM) plots of recursive residuals are given in Figure S3 of Supplementary Material for Case 1. Since all the points

are in-between confidence limits in all plots of Figure S3, the stability of the models is ensured. Then, we can proceed with drawing inferences from the ECM regression model and the cointegration equation following the modeling flow in Figure 3.

For Case 1, estimates of short-run coefficients and error correction (EC) coefficient of the ECM regression model in Equation (S2) of Supplementary Material are given in Table 5. According to the *F*-statistic, ECM is significant at the 1% significance level with a *p*-value of  $1.76 \times 10^{-6} < 0.01$ . Sunspot numbers and GHG emissions do not have a significant short-run effect on temperature anomalies. All the considered lags of short-run PV installation coefficients significantly affect the temperature anomalies, while the short-run effect of the PV installations series is insignificant. The value of the error correction coefficient is  $-0.760$ , and it is significant with a *p*-value close to zero. Thus, if temperature anomaly deviates from the long-run equilibrium relationship with GHG emissions, PV installations, and sunspot numbers, 76% of the non-equilibrium state will be adjusted in one quarter.

The cointegration equation was estimated as  $M_{t-1} = T_{t-1} - (0.0325E_{t-1} - 0.0520 \cdot \log(P_{t-1}) + 0.7143 \cdot \log(S_{t-1}))$ , where  $\pi_{TT} = -0.7604$  with  $(P = 4.55 \times 10^{-8} < 0.001)$  (see Section 2.6 of Supplementary Material for the details). The logic flow for the

use of the cointegration equation to draw inferences is explained in Figure 5. If a variable,  $X$ , is log-transformed, the coefficient of  $X$  is interpreted as predicted % change in the dependent variable for 1% change in  $X$  in the long-run. Otherwise, the coefficient of  $X$  is interpreted as the predicted change in the dependent variable for a one-unit change in  $X$  in the long-run.

**Table 5.** Estimates of the Short-Run Coefficients (in *Italic*) and the Error Correction Coefficient (in **Bold**) of the ECM for Case 1

| Variable                    | Coefficient   | Std. Error   | t-Statistic   | P-Value       |
|-----------------------------|---------------|--------------|---------------|---------------|
| $\omega'_E$                 | <i>-0.068</i> | <i>0.040</i> | <i>-1.702</i> | <i>0.094</i>  |
| $\omega'_P$                 | <i>0.047</i>  | <i>0.049</i> | <i>0.948</i>  | <i>0.347</i>  |
| $\psi'_P1$                  | <i>0.260</i>  | <i>0.064</i> | <i>4.078</i>  | <i>0.000*</i> |
| $\psi'_P2$                  | <i>0.323</i>  | <i>0.073</i> | <i>4.417</i>  | <i>0.000*</i> |
| $\psi'_P3$                  | <i>0.195</i>  | <i>0.071</i> | <i>2.769</i>  | <i>0.008*</i> |
| $\psi'_P4$                  | <i>0.209</i>  | <i>0.065</i> | <i>3.200</i>  | <i>0.002*</i> |
| $\psi'_P5$                  | <i>0.177</i>  | <i>0.056</i> | <i>3.186</i>  | <i>0.002*</i> |
| $\omega'_S$                 | <i>-0.065</i> | <i>0.219</i> | <i>-0.295</i> | <i>0.769</i>  |
| $\beta - EC$<br>coefficient | <b>-0.760</b> | <b>0.112</b> | <b>-6.764</b> | <b>0.000*</b> |

\* Significant at 1% level of significance.

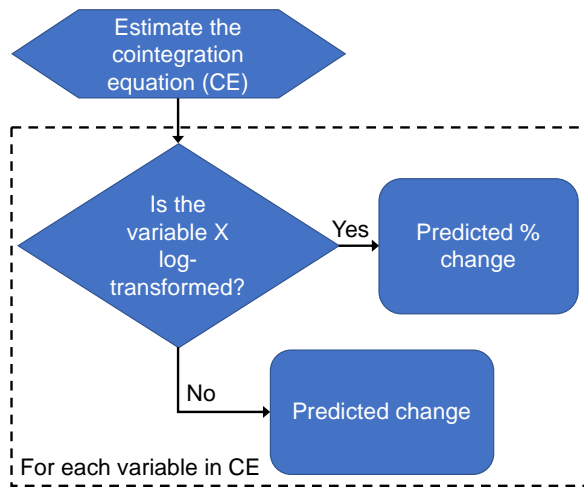


**Figure 5.** Use of the cointegration equation to draw inferences.

The potential amount of mitigation in temperature anomalies is calculated following the method diagram given in Figure 5. The estimates of long-run coefficients of GHG emissions, PV installations, and sunspot numbers are  $\pi_{TE} = 0.0325$ ,  $\pi_{TP} = -0.052$ , and  $\pi_{TS} = 0.7143$ , respectively. Since PV installations and sunspot numbers were log-transformed, while a 1% increase in PV installations has a 0.052% mitigating effect on the temperature anomalies in the long-run, a 1% increase in sunspot numbers increases temperature anomalies by 0.7143% in the long-run. From the coefficient of  $E_{t-1}$ , a unit increase in GHG emissions increases the temperature anomalies by 0.0325 °C in the long-run. Kristoufek (2017) also observed that sunspot numbers and global temperature levels have a stable relationship in time using a dataset between 1880 and 2016. However, they did not

report any quantitative information as provided in this article.

In order to make these figures more explicit, the transformation and the adjustment on the average PV installations series need to be taken back to the original scale. Due to the negative values in the adjusted average PV installations series, the log transformation was applied to the adjusted average PV installations series by  $\log(P_t + |\min(P_t)| + 0.1)$ , where  $|\min(P_t)| + 0.1 = 6,287.927$  (see Section 3.1), to shift it to the positive side of the real axis. The naïve forecast from the STL decomposition applied for the adjustment is 8.754. If  $P_t^*$  shows the raw average PV installations series, then the corresponding adjusted series is  $P_t = P_t^* - 8.754$  at any time point ahead,  $t$ . Writing  $P_t$  in its place in the log transformation, we get  $P_t^* - 8.754 + 6287.927 = P_t^* + 6279.173$ . So, if a naïve forecast for  $P_t^*$ , which is 20282, is used, then a 1% increase in  $P_t^* + 6279.173 = 20282 + 6279.173 = 26561.17$  corresponds to a 265.6117 kW increase in the raw average PV installations series. Given that the overall average of temperature anomalies series is 0.749, every 265.612 kW increase in average PV installations will mitigate temperature anomalies by  $3.893 \times 10^{-4}$  °C on average. The logic flow of this calculation is given in Figure S1 of Supplementary Material.

When the individual impact of sunspot numbers is investigated on the temperature anomalies without considering GHG emissions and PV installations, the optimal lags of the ARDL bounds test were specified as  $p_r = 1$  and  $p_s = 5$  (see Section 2.6 of the Supplementary Material). All residual diagnostics, including the insignificance of autocorrelation, homoscedasticity, and normality of the residuals, were confirmed, and no structure and stability issue was observed. For Cases 3, 4, and 5, there is not enough evidence to conclude the existence of cointegration between temperature anomalies and sunspot numbers even at a 10% level of significance. For Cases 1 and 2, it is only possible to observe a cointegration relationship at the 5% and 10% significance levels, respectively. For Cases 1 and 4, AICs are 126.49 and 127.15, respectively and BICs are 148.39 and 153.43, respectively. Although both AIC and BIC favour Case 1, which provides us with a significant test result at a 5% level of significance, AIC and BIC do not reflect a notable difference for Case 4, for which there is no evidence of a significant cointegration between temperature anomalies and sunspot numbers. Based on these results, it is not possible to strongly claim the existence of a long-run equilibrium between the pair of temperature anomalies and sunspot numbers. This observation is in accordance with the literature. GilAlana et al. (2014) reported a similar observation that both global temperatures and sunspot numbers show a long-run memory. However, there was not enough evidence to claim the existence of a cointegration relationship. Some authors have observed a possibility by correlating surface air temperatures with solar cycle length that solar activity may influence climate change. However, since correlation does not imply causality, there is no particular conclusion on this issue (Scott et al., 2003; Solanki and Krivova, 2003; Gray et al., 2010). From the causality perspective, an indication of Granger causality between temperature anomalies and sunspot numbers is observed in this study (Figure S2, Panel (e)). However, this is not backed up by the ARDL bounds testing.

**Table 6.** Results of ARDL Bounds Test for GHG Emissions, Residual Diagnostics Tests, AIC and BIC

|        | Critical values for the <i>F</i> -Test |              |              | <i>F</i> -Stat. | <i>P</i> -values of the tests for assumptions |       | GOF measures for the full model |        |
|--------|--|--------------|--------------|-----------------|---|-------|---------------------------------|--------|
|        | Sig. Level                             | <i>I</i> (0) | <i>I</i> (1) |                 |   |       |                                 |        |
| Case 1 | 10%                                    | 2.44         | 3.28         | 29.19*          | BG  | 0.699 | AIC                             | 231.16 |
|        | 5%                                     | 3.15         | 4.11         |                 | LB  | 0.975 | BIC                             | 240.16 |
|        | 1%                                     | 4.81         | 6.02         |                 | BP  | 0.746 |                                 |        |
|        |  |              |              |                 | SW  | 0.375 |                                 |        |
|        |  |              |              |                 | RESET   | 0.066 |                                 |        |

\* Significant at 1% level of significance.

### 3.4.2. GHG Emissions

Since it is observed that there are significant rolling correlations and Granger causality between GHG emissions and sunspot numbers, the same procedure as Section 3.4.1 is followed to test the existence of a cointegration relationship between these features (see Section 2.6.2 of Supplementary Material).

The lag orders were specified by optimizing AIC and BIC and simultaneously getting a stable model. The most parsimonious lag structure that gives a stable model was specified via BIC as  $p_E = 0$  and  $p_S = 0$  for the ARDL bounds test. When the test was run for Cases 1 to 5, only Case 1 ensured all the residual diagnostics. Recursive CUSUM and recursive MOSUM tests concluded the stability of the model. The results for the bounds test, residual diagnostics, and AIC and BIC are given in Table 6 for Case 1.

A significant long-run equilibrium relationship between GHG emissions and sunspot numbers is observed at a 1% level of significance. The error correction coefficient is  $-0.931$  with a  $p$ -value of  $7.74 \times 10^{-11} < 0.01$ . Thus, if GHG emissions deviate from their long-run equilibrium with sunspot numbers, 93% of the non-equilibrium state will be adjusted in one quarter. The short-run impact of sunspot numbers is insignificant. Since the cointegration equation is estimated as  $M_{t-1} = E_{t-1} - 0.0493 \cdot \log(S_{t-1})$ , a 1% increase in sunspot numbers increases GHG emissions by 0.0493% in the long-run. Thus, there is a significant but meager magnitude contribution from sunspot numbers to the increasing trends of GHG emissions.

## 4. Discussion and Conclusions

Almost all countries worldwide accept the phenomenon of climate change and its harmful impacts on nature. Some have already set their short- and long-run targets to mitigate the factors that aggravate climate change. Use of the solar PV generation for electricity production has a significant contribution to mitigating climate change. Therefore, this contribution needs to be revealed clearly to develop more accurate energy management plans and achievable targets. This article demonstrates the short- and long-run effects of solar energy utilization for electricity generation on the mean temperature anomalies by using autoregressive distributed lag models and bounds testing approaches. The dataset of interest includes quarterly mean temperature anomalies, quarterly mean GHG emissions, the average capacity of installed PV panels in Australia, and sunspot numbers between September 2001 and June 2019.

### 4.1. Relationship Patterns

The GHG emissions, average PV installations, and sunspot numbers individually Granger cause temperature anomalies. On the other hand, temperature anomalies Granger-cause neither GHG emissions nor average PV installations, as expected. A significant Granger causality between sunspot numbers and GHG emissions was not observed. A significant cointegration between temperature anomalies, anthropogenic GHG emissions, solar PV utilization, and solar cycle length was seen. Thus, climate change, anthropogenic GHG emissions, solar PV utilization, and solar cycle length exhibit a common movement pattern in the long-run, and at the equilibrium state, the distance between them remains constant. However, the short-run impacts of GHG emissions, average PV installations, and sunspot numbers on temperature anomalies are insignificant. This follows significant rolling correlations between temperature anomalies and GHG emissions, and temperature anomalies and average PV installations for seven quarters and insignificant rolling correlations for five quarters. By a cointegration coefficient of  $-0.76$ , the shocks to the equilibrium state are absorbed quickly, and 76% of the shock will be adjusted in one quarter; hence, a strong long-run relationship exists between the series. This implies that if the characteristics of some cointegrated series are changed, a considerable response from others, such as temperature anomalies, will be observed. Since we do not have control over solar cycle length, anthropogenic GHG emissions can be decreased and/or solar energy utilization can be increased by making appropriate political and energy management decisions to mitigate climate change.

### 4.2. Mitigation Potential

Our study showed that large PV installations have a solid capacity to mitigate temperature anomalies. A 1% increase in average PV installations helps to reduce the temperature anomalies by 0.052%. In order to make it clearer in practice, if the increasing trend in average PV installations persists, for example, as in the first and second quarters of 2011, where there was a 20830.67 kW increase, the increasing temperature can be reduced by 0.0305 °C in one quarter. These figures demonstrate that it is very critical to increase solar energy usage by PV installations to mitigate the temperature anomalies. Considering the immense impacts of slight increases in global mean temperature on nature, the gain by allocating more resources to solar energy investments is extremely crucial. From the rolling correlation analysis and ARDL bounds testing results, it is high-

ly likely to see a considerable decrease in the temperature anomalies, especially after large-scale PV installations.

Most countries formulate their climate change targets in terms of reduction in GHG emissions and compare their reduction percentages over the years to other countries' performance (for example, DEE, 2019). However, this does not translate into the impact of the reduction on climate change. As another practical use of our results, the impact of the solar PV capacity installations on temperature anomalies was observed as every 265.6117 kW increase in average PV installations mitigates temperature anomalies by  $3.893 \times 10^{-4}$  °C on average. This quantitative information has the potential to contribute to scenario-based studies on the reduction of GHG emissions, such as the recent study by Jäger-Waldau et al. (2020).

#### 4.3. Impact of Solar Activity

There were discussions around the significance of solar activity on global warming in the literature (Solanki and Krivova, 2003; Reimer, 2004). Remier (2004) mentioned that solar activity has no role in global warming. On the other hand, Roy (2018) stated that the solar cycle would contribute to the decline in the sea ice around the Arctic, which was also linked to CO<sub>2</sub> emissions by Notz and Stroeve (2016). Another important conclusion of this study is about the impact of solar cycle length on temperature anomalies. A 1% increase in sunspot numbers increases temperature anomalies in Australia by 0.71% in the long-run. This observation confirms Friis-Christensen and Lassen (1991) and Lassen and Friis-Christensen (1995). There is also a significant but low-magnitude long-run relationship between GHG emissions and sunspot numbers. Quantitatively, it is estimated to see a 0.0493% increase in GHG emissions for each 1% increase in sunspot numbers. This finding introduces a default increment/decrement into the temperature anomalies and GHG emissions by increasing/decreasing sunspot numbers. Although the numerical impact of sunspot numbers on GHG emissions is not sufficient to claim that increasing GHG emissions can be attributed to solar forcing rather than anthropogenic activities, it is recommended that the studies on the effect of anthropogenic CO<sub>2</sub> or GHG emissions on climate change consider the confounding effect of solar cycle length and GHG emissions, and filtrate/consider it before drawing conclusions on the significance and the amount of the effect of GHG emissions on the climate change.

#### 4.4. Generalizability and Limitations

Our modeling framework was implemented using Australian data, but this framework is a universal modeling framework for any other location or set of dependent and exploratory features. The generalizability of the results obtained with Australian data to other locations depends on similarities and differences between the locations in temperature anomalies, GHG emissions, and solar energy potential. Sunspot numbers are independent of location. Most of the globe has similar temperature anomalies characteristics as Australia except far northern parts of Asia and North America (NOAA, 2020). GHG emis-

sions show a considerable variation over the countries (Olivier and Peters, 2021). While installed PV capacity is universal, the efficiency of PV panels depends on the location. In this sense, for countries with a similar carbon footprint and a lower solar energy potential than Australia, our results provide upper limits of reduction in temperature anomalies per percent increase in PV utilization for electricity generation. On the other hand, our results give lower limits for the countries with a similar carbon footprint and a higher solar energy potential than Australia.

One of the limitations of this study is the length of the series used for the analysis. Considering that solar energy utilization for electricity generation is a relatively new issue and started to follow an explosive trend after 2011 in Australia, the series used in the study included almost all the available information on this matter. In this sense, the obtained results take all available information into account. In this study, only PV installations were focused on among other forms of solar energy usage. The increasing trend in the share of solar PV generation is the main reason for this. Since the residual diagnostics demonstrate that there was no excess autocorrelation left in the model, the inclusion of another series into ARDL testing is not required in terms of the generalizability of the results. Since the impact of other solar energy systems will add up on the mitigating potential of PV systems, the figures presented in this study can be taken as a baseline potential of solar energy utilization. Another limitation is that the installed capacity cannot be fully utilized in many countries. To carry on the cointegration analysis in this study, we need to have all the covariates measured simultaneously from 2001 to 2019. It is possible to get live energy generation data from the installed PV network via the Australian PV Institute. However, in this case, it is not possible to include other covariates since they are not available at the same frequency. On the other hand, it is not quite possible to aggregate the ultra-high frequency live PV generation data to get a quarterly series that dates back to 2001. Here, the trade-off is either getting a very short time series based on aggregated live data or working with a longer series by taking available PV installation data. Since longer series were needed to run time series analyses, installed PV capacity data were used knowing that the utilization is not 100%. However, installed PV capacity still provides us with information about solar energy utilization for electricity generation, assuming that PV devices are installed at optimum settings for efficiency.

**Acknowledgments.** The author would like to thank five reviewers for their valuable comments and suggestions that considerably improved the clarity and quality of the article.

#### References

- Abdullah, M.A., Agalgaonkar, A.P. and Muttaqi, K.M. (2014). Climate change mitigation with integration of renewable energy resources in the electricity grid of New South Wales, Australia. *Renew. Energ.*, 66, 305-313. <https://doi.org/10.1016/j.renene.2013.12.014>
- Akaike, H. (1970). Statistical predictor identification. *Ann. Inst. Stat. Math.*, 22, 203-217. <https://doi.org/10.1007/BF02506337>
- Asteriou, D. and Hall, S.G. (2021). *Applied Econometrics*. 4th ed., Macmillan International Higher Education, New York. ISBN: 9781

- 352012033
- Australian Government Bureau of Meteorology (BOM, 2021a). Climate Change – Trends and Extremes Database. <http://www.bom.gov.au/climate/change/> (accessed December 9, 2021).
- Australian Government Bureau of Meteorology (BOM, 2021b). Climate Change and Variability Database. [http://www.bom.gov.au/web/01/ncc/www/cli\\_chg/timeseries/tmean/allmonths/aus/latest.txt/](http://www.bom.gov.au/web/01/ncc/www/cli_chg/timeseries/tmean/allmonths/aus/latest.txt/) (accessed December 9, 2021).
- Australian Government Department of the Environment and Energy (DEE, 2019). Australia's Fourth Biennial Report, Commonwealth of 2019. <https://www.environment.gov.au/climatechange/publications/australias-fourth-biennial-report/> (accessed February 27, 2020).
- Australian Government Department of Industry, Science, Energy and Resources (DI, 2018). The Renewable Energy Target Scheme. <http://www.environment.gov.au/climate-change/government/renewable-energy-target-scheme/> (accessed December 13, 2018).
- Australian Government Department of Industry, Science, Energy and Resources (DI, 2019). Australian Greenhouse Emissions Information System. <http://ageis.climatechange.gov.au/> (accessed December 13, 2019).
- Australian Government Department of Industry, Science, Energy and Resources (DI, 2021a). Australian Energy Statistics. <https://www.energy.gov.au/data/renewables/> (accessed October 11, 2021).
- Australian Government Department of Industry, Science, Energy and Resources (DI, 2021b). National Greenhouse Gas Inventory Quarterly Update: March 2021. <https://www.industry.gov.au/data-and-publications/national-greenhouse-gas-inventory-quarterly-update-march-2021/> (accessed October 11, 2021).
- Australian Government Department of Industry, Science, Energy and Resources (DI, 2021c). Quarterly Update of Australia's National Greenhouse Gas Inventory: June 2019. Commonwealth of Australia 2019. <https://www.industry.gov.au/data-and-publications/nationalgreenhouse-gas-inventory-june-2019/> (accessed December 09, 2021).
- Australian PV Institute (2021). Australian PV installations since April 2001. <http://pv-map.apvi.org.au/analyses/> (accessed December 9, 2021).
- Ayers, G.P. (2017). Lower tropospheric temperatures 1978-2016: The role played by anthropogenic global warming. *J. South. Hemisph. Earth Syst. Sci.*, 67(1), 2-11. <https://doi.org/10.1071/ES17002>
- Bahadori, A. and Nwaoha, C. (2013). A review on solar energy utilisation in Australia. *Renew. Sustain. Energy Rev.*, 18, 1-5. <https://doi.org/10.1016/j.rser.2012.10.003>
- Banerjee, A., Dolado, J.J., Galbraith, J.W. and Hendry, D. (1993). *Co-Integration, Error Correction, and the Econometric Analysis of NonStationary Data*. Oxford University Press. ISBN: 9780198288107
- Beenstock, M., Reingewertz, Y. and Paldor, N. (2012). Polynomial cointegration tests of anthropogenic impact on global warming. *Earth Syst. Dyn.*, 3(2), 173-188. <https://doi.org/10.5194/esd-3-173-2012>
- Booth, R.J. (2018). On the influence of solar cycle lengths and carbon dioxide on global temperatures. *J. Atmos. Sol. Terr. Phys.*, 173, 96-108. <https://doi.org/10.1016/j.jastp.2018.01.026>
- Breyer, C., Koskinen, O. and Blechinger, P. (2015). Profitable climate change mitigation: The case of greenhouse gas emission reduction benefits enabled by solar photovoltaic systems. *Renew. Sustain. Energy Rev.*, 49, 610-628. <https://doi.org/10.1016/j.rser.2015.04.061>
- Bruns, S.B. and Stern, D.I. (2019). Lag length selection and p-hacking in Granger causality testing: Prevalence and performance of meta-regression models. *Empir. Econ.*, 56(3), 797-830. <https://doi.org/10.1007/s00181-018-1446-3>
- Creutzig, F., Agoston, P., Goldschmidt, J.C., Luderer, G., Nemet, G. and Pietzcker, R.C. (2017). The underestimated potential of solar energy to mitigate climate change. *Nat. Energy*, 2(9), 1-9. <https://doi.org/10.1038/nenergy.2017.140>
- Cryer, J.D. and Chan, K. (2008). *Time Series Analysis with Applications in R*. 2nd ed., Springer, New York. <https://doi.org/10.1007/978-0-387-75959-3>
- Davis, W.J. (2017). The relationship between atmospheric carbon dioxide concentration and global temperature for the last 425 million years. *Climate*, 5(4), 76. <https://doi.org/10.3390/cli5040076>
- Demirhan, H. (2020). dLagM: An R package for distributed lag models and ARDL bounds testing. *PLoS ONE*, 15(2), e0228812. <https://doi.org/10.1371/journal.pone.0228812>
- Elkadhi, H., Kalai, M. and Ben Hamida, R. (2017). The relationship between energy consumption, greenhouse gas emissions, and meteorological factors in Sfax (Tunisia): An ARDL bounds testing approach. *J. Environ. Econ. Policy*, 6(3), 309-323. <https://doi.org/10.1080/21606544.2017.1300108>
- Elum, Z.A. and Momodu, A.S. (2017). Climate change mitigation and renewable energy for sustainable development in Nigeria: A discourse approach. *Renew. Sustain. Energy Rev.*, 76, 72-80. <https://doi.org/10.1016/j.rser.2017.03.040>
- Emodi, N.V., Chaiechi, T. and Alam Beg, A.R. (2018). The impact of climate change on electricity demand in Australia. *Energy Environ.*, 29(7), 1263-1297. <https://doi.org/10.1177/0958305X18776538>
- Esen, H., Esen, M. and Ozsolak, O. (2017). Modelling and experimental performance analysis of solar-assisted ground source heat pump system. *J. Exp. Theor. Artif. In.*, 29(1), 1-17. <https://doi.org/10.1080/0952813X.2015.1056242>
- Fierro, A.O. and Leslie, L.M. (2014). Relationships between southeast Australian temperature anomalies and large-scale climate drivers. *J. Clim.*, 27(4), 1395-1412. <https://doi.org/10.1175/JCLI-D-1300229.1>
- Friis-Christensen, E. and Lassen, K. (1991). Length of the solar cycle: An indicator of solar activity closely associated with climate. *Science*, 254, 698-700. <https://doi.org/10.1126/science.254.5032.698>
- Gershunov, A., Schneider, N. and Barnett, T. (2001). Low-frequency modulation of the ENSO Indian monsoon rainfall relationship: Signal or noise? *J. Clim.*, 14(11), 2486-2492. [https://doi.org/10.1175/1520-0442\(2001\)014<2486:LFMOT>2.0.CO;2](https://doi.org/10.1175/1520-0442(2001)014<2486:LFMOT>2.0.CO;2)
- Gil-Alana, L.A., Yaya, O.S. and Shittu, O.I. (2014). Global temperatures and sunspot numbers. Are they related? *Phys. A: Stat. Mech. Appl.*, 396, 42-50. <https://doi.org/10.1016/j.physa.2013.10.043>
- Granger, C.W.J. (1969). Investigating causal relations by econometric models and cross-spectral methods. *Econometrica*, 37(3), 424-438. <https://doi.org/10.1017/CBO9780511753978.002>
- Gray, L.J., Beer, J., Geller, M., Haigh, J.D., Lockwood, M., Matthes, K., Cubasch, U., Fleitmann, D., Harrison, G., Hood, L. Luterbacher, J., Meehl, G.A., Shindell, D., van Geel, B., and White, W. (2010). Solar influences on climate. *Rev. Geophys.*, 48(4), 1-53. <https://doi.org/10.1029/2009RG000282>
- Geweke, J. and Meese, R. (1981). Estimating regression models of finite but unknown order. *Int. Econ. Rev.*, 22, 55-70. <https://doi.org/10.2307/2526135>
- Hébert, R., and Lovejoy, S. (2018). Regional climate sensitivity- and historical-based projections to 2100. *Geophys. Res. Lett.*, 45(9), 4248-4254. <https://doi.org/10.1002/2017GL076649>
- Hyndman, R.J. and Athanasopoulos, G. (2018). *Forecasting: Principles and Practice*. 2nd ed, OTexts, Melbourne, Australia. ISBN: 9780987507112
- International Energy Agency (IEA, 2021). Solar PV. <https://www.iea.org/reports/solar-pv/> (accessed December 15, 2021).
- Jäger-Waldau, A., Kougiyas, I., Taylor, N. and Thiel, C. (2020). How photovoltaics can contribute to GHG emission reductions of 55% in the EU by 2030. *Renew. Sustain. Energy Rev.*, 126, 109836. <https://doi.org/10.1016/j.rser.2020.109836>
- Kristoufek, L. (2017). Has global warming modified the relationship between sunspot numbers and global temperatures? *Phys. A: Stat. Mech. Appl.*, 468, 351-358. <https://doi.org/10.1016/j.physa.2016.10.089>
- Kwiatkowski, D., Phillips, P.C., Schmidt, P. and Shin, Y. (1992). Testing the null hypothesis of stationarity against the alternative of a unit root: How sure are we that economic time series have a unit

- root? *J. Econom.*, 54(1-3), 159-178. [https://doi.org/10.1016/0304-4076\(92\)90104-Y](https://doi.org/10.1016/0304-4076(92)90104-Y)
- Lassen, K. and Friis-Christensen, E. (1995). Variability of the solar-cycle length during the past five centuries and the apparent association with terrestrial climate. *J. Atmos. Sol. Terr. Phys.*, 57, 835-845. [https://doi.org/10.1016/0021-9169\(94\)00088-6](https://doi.org/10.1016/0021-9169(94)00088-6)
- Lassen, K. and Friis-Christensen, E. (2000). Reply to the article "solar cycle lengths and climate: a reference revisited". *J. Geophys. Res.*, 105 (A12), 27493-27495. <https://doi.org/10.1029/2000JA900067>
- Li, Q., Sun, W., Huang, B., Dong, W., Wang, X., Zhai, P., and Jones, P. (2020). Consistency of global warming trends strengthened since 1880s. *Sci. Bull.*, 65(20), 1709-1712. <https://doi.org/10.1016/j.scib.2020.06.009>
- Masson, V., Bonhomme, M., Salagnac, J.L., Briottet, X. and Lemonsu, A. (2014). Solar panels reduce both global warming and urban heat island. *Front. Environ. Sci.*, 2(14). <https://doi.org/10.3389/fenvs.2014.00014>
- Muryshev, K.E., Eliseev, A.V., Mokhov, I.I. and Timazhev, A.V. (2017). Lead-lag relationships between global mean temperature and the atmospheric CO<sub>2</sub> content in dependence of the type and time scale of the forcing. *Glob. Planet. Change*, 148, 29-41. <https://doi.org/10.1016/j.gloplacha.2016.11.005>
- NOAA National Centers for Environmental Information (NOAA, 2020). State of the Climate: Global Climate Report for Annual 2020. <https://www.ncdc.noaa.gov/sotc/global/202013> (accessed October 7, 2021).
- NOAA National Centers for Environmental Information (NOAA, 2021). Global Atmospheric Carbon Dioxide and Surface Temperature. <https://www.climate.gov/media/13840> (accessed December 14, 2021).
- Notz, D. and Stroeve, J. (2016). Observed Arctic sea-ice loss directly follows anthropogenic CO<sub>2</sub> emission. *Science*, 354(6313), 747-750. <https://doi.org/10.1126/science.aag2345>
- Olivier, J.G.J. and Peters, J.A.H.W. (2020). *Trends in Global CO<sub>2</sub> and Total Greenhouse Gas Emissions; 2020 Report*. PBL Netherlands Environmental Assessment Agency.
- Parzen, E. (1982). ARARMA models for time series analysis and forecasting. *J. Forecast.*, 1(1), 67-82. <https://doi.org/10.1002/for.3980010108>
- Perez, I.A., Sánchez, M.L., García, M.Á., Pardo, N. and Fernández-Duque, B. (2018). The influence of meteorological variables on CO<sub>2</sub> and CH<sub>4</sub> trends recorded at a semi-natural station. *J. Environ. Manage.*, 209, 37-45. <https://doi.org/10.1016/j.jenvman.2017.12.028>
- Pesaran, M.H., Shin, Y. and Smith, R.J. (2001). Bounds testing approaches to the analysis of level relationships. *J. Appl. Econ.*, 16(3), 289-326. <https://doi.org/10.1002/jae.616>
- Pfaff, B. (2008). *Analysis of Integrated and Cointegrated Time Series with R*. 2nd ed., Springer, New York. ISBN: 9780387759661
- Pretis, F. and Hendry, D.F. (2013). Comment on "Polynomial cointegration tests of anthropogenic impact on global warming" by Beenstock et al. (2012) - some hazards in econometric modelling of climate change. *Earth Syst. Dynam.*, 4(2), 375-384. <https://doi.org/10.5194/esd-4-375-2013>
- Reimer, P. (2004). Spots from rings. *Nature*, 431, 1047-1048. <https://doi.org/10.1038/4311047a>
- Roy, I. (2018). Solar cyclic variability can modulate winter Arctic climate. *Sci. Rep.*, 8(1), 4864. <https://doi.org/10.1038/s41598-018-22854-0>
- Said, S.E. and Dickey, D.A. (1984). Testing for unit roots in autoregressive-moving average models of unknown order. *Biometrika*, 71(3), 599-607. <https://doi.org/10.1093/biomet/71.3.599>
- Shahsavari, A. and Akbari, M. (2018). Potential of solar energy in developing countries for reducing energy-related emissions. *Renew. Sustain. Energy Rev.*, 90, 275-291. <https://doi.org/10.1016/j.rser.2018.03.065>
- Singh, D., Singh, R.P., Singh, A.K., Kulkarni, M.N., Gautam, A.S. and Singh, A.K. (2011). Solar activity, lightning and climate. *Surv. geophys.*, 32(6), 659. <https://doi.org/10.1007/s10712-011-9127-1>
- Solanki, S.K. and Krivova, N.A. (2003). Can solar variability explain global warming since 1970? *J. Geophys. Res. Space Phys.*, 108(A5). <https://doi.org/10.1029/2002JA009753>
- Solheim, J.E., Stordahl, K. and Humlum, O. (2012). The long sunspot cycle 23 predicts a significant temperature decrease in cycle 24. *J. Atmos. Sol. Terr. Phys.*, 80, 267-284. <https://doi.org/10.1016/j.jastp.2012.02.008>
- SWPC NOAA (2021). Solar Cycle Progression. <https://www.swpc.noaa.gov/products/solar-cycle-progression/> (accessed December 9, 2021)
- Scott, P.A., Jones, G.S. and Mitchell, J.F. (2003). Do models underestimate the solar contribution to recent climate change? *J. Clim.*, 16(24), 4079-4093. [https://doi.org/10.1175/1520-0442\(2003\)016<4079:DMUTSC>2.0.CO;2](https://doi.org/10.1175/1520-0442(2003)016<4079:DMUTSC>2.0.CO;2)
- Susskind, J., Schmidt, G.A., Lee, J.N. and Iredell, I. (2019). Recent global warming as confirmed by AIRS. *Environ. Res. Lett.*, 14, 044030. <https://doi.org/10.1088/1748-9326/aafd4e>
- Thornton, D.L. and Batten, D.S. (1985). Lag-Length Selection and Tests of Granger Causality Between Money and Income. *J. Money Credit Bank.*, 17(2), 164-178. <https://doi.org/10.2307/1992331>
- Tsoutsos, T., Frantzeskaki, N. and Gekas, V. (2005). Environmental impacts from the solar energy technologies. *Energy Policy*, 33(3), 289-296. [https://doi.org/10.1016/S0301-4215\(03\)00241-6](https://doi.org/10.1016/S0301-4215(03)00241-6)
- Valipour, M., Bateni, S.M. and Jun, C. (2021). Global surface temperature: A new insight. *Climate*, 9(5), 81. <https://doi.org/10.3390/cli9050081>
- Zeileis A. and Hothorn, T. (2002). Diagnostic checking in regression relationships. *R News*, 2(3), 7-10. [https://www.rproject.org/doc/Rnews/Rnews\\_2002-3.pdf](https://www.rproject.org/doc/Rnews/Rnews_2002-3.pdf)
- Zhai, S., Song, G., Qin, Y., Ye, X. and Lee, J. (2017). Modeling the impacts of climate change and technical progress on the wheat yield in inland China: An autoregressive distributed lag approach. *PLoS ONE*, 12(9), e0184474. <https://doi.org/10.1371/journal.pone.0184474>
- Zhang, C., Sun, J., Lubell, M., Qiu, L. and Kang, K. (2019). Design and simulation of a novel hybrid solar-biomass energy supply system in northwest China. *J. Clean. Prod.*, 233, 1221-1239. <https://doi.org/10.1016/j.jclepro.2019.06.128>